PLOS ONE

High-throughput phenotyping analysis of maize at the seedling stage using end-to-end segmentation network
--Manuscript Draft--

Manuscript Number:	PONE-D-20-32300
Article Type:	Research Article
Full Title:	High-throughput phenotyping analysis of maize at the seedling stage using end-to-end segmentation network
Short Title:	High-throughput phenotyping analysis of seedling maize
Corresponding Author:	Weiliang Wen National Engineering Research Center for Information Technology in Agriculture Beijing, Beijing CHINA
Keywords:	maize; deep learning; top-view; image segmentation; phenotype extraction
Abstract:	Image processing technologies are available for high-throughput acquisition and analysis of phenotypes for crop populations, which is of great significance for crop growth monitoring, evaluation of seedling condition, and cultivation management. However, existing methods rely on empirical segmentation thresholds, thus can have insufficient accuracy of extracted phenotypes. Taking maize as an example crop, we propose a phenotype extraction approach from top-view images at the seedling stage. An end-to-end segmentation network, named PlantU-net, which uses a small amount of training data, was explored to realize automatic segmentation of top-view images of a maize population at the seedling stage. Morphological and color related phenotypes were automatic extracted, including maize shoot coverage, circumscribed radius, aspect ratio, and plant azimuth plane angle. The results show that the approach can segment the shoots at the seedling stage from top-view images, obtained either from the UAV or ground high-throughput phenotyping platform. The average segmentation accuracy, recall rate, and F1 score are 0.96, 0.98, and 0.97, respectively. The extracted phenotypes, including maize shoot coverage, circumscribed radius, aspect ratio, and plant azimuth plane angle, are highly correlated with manual measurements (R^2 =0.96-0.99). This approach requires less training data and thus has better expansility. It provides practical means for high-throughput phenotyping analysis of early growth stage crop populations.
Order of Authors:	Yinglun Li
	Weiliang Wen
	Xinyu Guo
	Zetao Yu
	Shenghao Gu
	Haipeng Yan
	Chunjiang Zhao
Additional Information:	
Question	Response
Financial Disclosure Enter a financial disclosure statement that describes the sources of funding for the work included in this submission. Review the submission guidelines for detailed requirements. View published research articles from _PLOS ONE_ for specific	

examples.

This statement is required for submission and **will appear in the published article** if the submission is accepted. Please make sure it is accurate.

* typeset

Competing Interests

Use the instructions below to enter a competing interest statement for this submission. On behalf of all authors, disclose any competing interests that could be perceived to bias this work—acknowledging all financial support and any other relevant financial or non-financial competing interests.

This statement **will appear in the published article** if the submission is accepted. Please make sure it is accurate. View published research articles from *PLOS ONE* for specific examples.

The authors have declared that no competing interests exist.

NO authors have competing interests

Enter: *The authors have declared that no competing interests exist*.

Authors with competing interests

Enter competing interest details beginning with this statement:

I have read the journal's policy and the authors of this manuscript have the following competing interests: [insert competing interests here]

Ethics Statement

Enter an ethics statement for this submission. This statement is required if the study involved:

• Human participants
• Human specimens or tissue
• Vertebrate animals or cephalopods
• Vertebrate embryos or tissues
• Field research

Write "N/A" if the submission does not require an ethics statement.

General guidance is provided below. Consult the submission guidelines for detailed instructions. **Make sure that all information entered here is included in the Methods section of the manuscript.**

N/A

Data Availability

Authors are required to make all data underlying the findings described fully available, without restriction, and from the time of publication. PLOS allows rare exceptions to address legal and ethical concerns. See the PLOS Data Policy and FAQ for detailed information.

Yes - all data are fully available without restriction

A Data Availability Statement describing where the data can be found is required at submission. Your answers to this question constitute the Data Availability Statement and **will be published in the article**, if accepted.

Important: Stating 'data available on request from the author' is not sufficient. If your data are only available upon request, select 'No' for the first question and explain your exceptional situation in the text box.

Do the authors confirm that all data underlying the findings described in their manuscript are fully available without restriction?

Describe where the data may be found in full sentences. If you are copying our sample text, replace any instances of XXX with the appropriate details.

- If the data are **held or will be held in a public repository**, include URLs, accession numbers or DOIs. If this information will only be available after acceptance, indicate this by ticking the box below. For example: *All XXX files are available from the XXX database (accession number(s) XXX, XXX.).*
- If the data are all contained **within the manuscript and/or Supporting Information files**, enter the following: *All relevant data are within the manuscript and its Supporting Information files.*
- If neither of these applies but you are able to provide **details of access elsewhere**, with or without limitations, please do so. For example:

  Data cannot be shared publicly because of [XXX]. Data are available from the XXX Institutional Data Access / Ethics Committee (contact via XXX) for researchers who meet the criteria for access to confidential data.

  The data underlying the results presented in the study are available from (include the name of the third party

All relevant data are within the manuscript and its Supporting Information files

and contact information or URL). • This text is appropriate if the data are owned by a third party and authors do not have permission to share the data. * typeset	
Additional data availability information:	Tick here if your circumstances are not covered by the questions above and you need the journal's help to make your data available.

1 # High-throughput phenotyping analysis of maize at the
2 # seedling stage using end-to-end segmentation network

3 Yinglun Li [1,2], Weiliang Wen [2,3*] , Xinyu Guo [2,3], Zetao Yu [3] , Shenghao Gu [2,3], Haipeng

4 Yan [4] and Chunjiang Zhao [1,2,3*]

5 [1] College of Resources and Environment, Jilin Agricultural University, Changchun
6 130118, China
7 [2] Beijing Research Center for Information Technology in Agriculture, Beijing
8 100097, China
9 [3] Beijing Key Lab of Digital Plant, National Engineering Research Center for
10 Information Technology in Agriculture, Beijing 100097, China
11 [4] Beijing Shunxin Agricultural Science and Technology Co., Ltd, Beijing 100097,
12 China
13 * wlwen37@163.com(WW); zhaocj@nercita.org.cn(CZ)

14 # Abstract

15 Image processing technologies are available for high-throughput acquisition and
16 analysis of phenotypes for crop populations, which is of great significance for crop
17 growth monitoring, evaluation of seedling condition, and cultivation management.
18 However, existing methods rely on empirical segmentation thresholds, thus can have
19 insufficient accuracy of extracted phenotypes. Taking maize as an example crop, we
20 propose a phenotype extraction approach from top-view images at the seedling stage.
21 An end-to-end segmentation network, named PlantU-net, which uses a small amount
22 of training data, was explored to realize automatic segmentation of top-view images of
23 a maize population at the seedling stage. Morphological and color related phenotypes
24 were automatic extracted, including maize shoot coverage, circumscribed radius, aspect
25 ratio, and plant azimuth plane angle. The results show that the approach can segment
26 the shoots at the seedling stage from top-view images, obtained either from the UAV
27 or ground high-throughput phenotyping platform. The average segmentation accuracy,
28 recall rate, and F1 score are 0.96, 0.98, and 0.97, respectively. The extracted
29 phenotypes, including maize shoot coverage, circumscribed radius, aspect ratio, and
30 plant azimuth plane angle, are highly correlated with manual measurements (R^2=0.96-
31 0.99). This approach requires less training data and thus has better expansibility. It
32 provides practical means for high-throughput phenotyping analysis of early growth
33 stage crop populations.
34 **Keywords:** maize, deep learning, top-view, image segmentation, phenotype extraction

35

36

Introduction

Recently, plant phenotyping has become a rapidly developing data-intensive discipline [1,2]. Studying the phenotypic information of plants under different environmental conditions provides insight into plant genetics [3,4] and is important identifying and evaluating the phenotypic differences of different cultivars [5]. Field phenotypes are the manifestation of crop growth under real conditions and are an important basis for genetic screening and the identification of mutations in field crops [6]. Therefore, it is important to conduct analyses of crop phenotypes under field conditions with high-precision. Traditionally, field phenotypic traits were obtained by manually measuring traits, which is work-intensive and time-consuming, limiting the number of measurable phenotypic traits. The development of information technology has made it possible to automatically acquire multi-source data of crops using high-throughput technology, such as images, point clouds, and spectrally collected data in the field, which can greatly reduce the manual labor and time commitment required to obtain crop phenotypic information. The cost of point cloud and spectral data acquisition sensors are more expensive than the image sensors; thus, image-based plant phenotyping has become a hot topic in agricultural research in recent years [7].

Unmanned aerial vehicles (UAVs), manned ground vehicles (MGVs), and tractor-based high-throughput phenotyping platforms (HTPPs) can rapidly obtain high-resolution top-view images of crop canopies. Researchers can extract phenotypic parameters [8], such as plant size [9], shape [10], and color [11], from the acquired images. For some specific phenotypic parameters, these approaches can be substituted for traditional manual measurements, improving the efficiency of collecting plant phenotypic information. However, different data collection methods and different environments can generate inconsistent image data. Thus, reliable automated methods are needed to extract accurate phenotypic information from large, complex datasets. Recently, researchers have proposed a variety of algorithms to address the above problems [12,13]; the basis of these algorithms is image segmentation.

Accurate and efficient field crop image segmentation methods can rapidly and accurately obtain crop phenotypic traits. Researchers have conducted numerous studies on the image segmentation of crops under field conditions [15,16]. Early field crop image segmentation methods can be roughly divided into four categories: shape constraints [17], edge detection [18], deep information integration [19], and machine learning methods [20]. These studies can address issues in the field, such as disease identification [21,22], environmental stress [23], chlorophyll diagnosis [24], and phenotypic extraction [25], at the individual plant or population scale. However, the background of the plant images in these methods was manually constructed or relatively simple. In addition, these methods typically have strict requirements on the light intensity of the input images.

With its powerful feature extraction capabilities, deep learning technology is a

turning point for accurately and rapidly addressing image segmentation problems [26,27]. Fully trained models can achieve accurate image segmentation for regions of interest (ROI). Currently, popular deep neural network processing methods use center point detection [28]. Alternately, deep neural network processing methods directly perform leaf edge detection [29] to achieve image segmentation and whole or partial segmentation of images of plants collected under field [26] or indoor [30] conditions. Segmentation results are used to extract crop features [31], as well as quantify [30,32], count [11], and estimate diseases [33,34]. Deep learning has advantages in collaborative applications such as the interactions between genotype and environment. Compared with classical methods, deep learning technology does not rely on manual filters and feature annotations; instead, it learns the best representation of the data, allowing it to perform better in scenarios where the amount of data is sufficient.

Researchers have applied advanced hardware facilities and intelligent data processing methods to research plant phenotypes. However, accurate extraction of fine-scale phenotypic information of individual plants is still difficult under field conditions because of the occlusion and crossover that occurs in the later growth stages of crops. In a field maize population, for example, leaves of adjacent shoots appear cross-shaded after ridging, which makes it difficult to completely and precisely extract the phenotypes of individual plants within a population. Therefore, obtaining and resolving phenotypic traits of maize shoots at the seedling stage is a better way to characterize the phenotypic traits of individual plants, and can guide the structural-functional analysis of maize populations in later growth stages. For example, phenotypic traits at the seedling stage provide reference information, such as growth position, direction, and growth potential, for each shoot within the population.

In this paper, a full convolutional neural network based end-to-end image segmentation approach of maize population at the seedling stage, named PlantU-net, is proposed. Using this approach, each shoot within the population image is precisely localized and the phenotypes are extracted. The approach is expected to provide technical support for image processing and high-throughput phenotype extraction from the top-view images acquired by UAVs and field phenotyping platforms.

Materials and Methods

Data Acquisition

Data for PlantU-net model training and inbred line population analysis were obtained at the experimental field, Beijing Academy of Agriculture and Forestry Sciences, Beijing, China (39°56′ N, 116°16′ E). A population used for correlation analysis with 502 cultivars [36] was planted in the field on May 17, 2019. The row and plant spacing were 60 and 27.8 cm, respectively. The planted cultivars can be divided

into four subpopulations [36]: hard stalks (SS), non-hard stalks (NSS), tropical and subtropical (TST), and mixed inbred lines (Mixed), with 32, 139, 221, and 110 cultivars for each subpopulation. Top-view images of shoots were obtained 12 (V3) and 26 (V6) days after sowing. Images were acquired using an EOS5DIII digital camera with a 24–70 mm lens vertically downward mounted on a SLR tripod (height 1.7 m, as shown in Figure 1a), with each image containing approximately five to six plants. Size-known markers are placed in the original image to provide a scale reference for later image cropping and scaling. When acquiring the images, the experimenter faced to east, ensuring that the left side of the captured images was oriented to the north. Image acquisition occurred over three days (one day for V3; two days for V6): one sunny day for V3, and one sunny and one cloudy day for V6. The incident light angle and the intensity differed over the course of data acquisition. Drip irrigation belts were arranged to ensure adequate water and fertilizer. Consequently, these changes in the background cause challenges for later image processing. Top-view images of maize populations at the seedling stage were obtained using UAV and a field phenotyping platform.

The experimental plots of the field phenotyping platform were adjacent to the plots obtained from the above-mentioned model dataset and managed in the same manner. Thirteen maize hybrids were planted within the coverage of the platform on May 25, 2019; this included one row of each hybrid, with 1.5 m long rows and 60 cm row spacing. The platform's image acquisition system consisted of a stable imaging chamber and a Hikari MV-CA060-10GC color camera. The camera lens was 2.5 m above the ground, and the resolution of the captured images was 3072×2048 pixels. In the process of data acquisition, the imaging chamber was equipped with a lens that moved in an S-shaped trajectory above the experimental plot, and the acquired images were stitched together to obtain a complete top-view image of the plot. The data acquisition of the ground phenotyping platform is shown in Figure 1b. The image acquired on the 17th day after sowing was selected for subsequent phenotypic analysis.

The experiment of top-view image data acquisition using UAV of maize populations at the seedling stage was carried out at the Tongzhou Experimental Field, Beijing Academy of Agricultural and Forestry Sciences (39°70′ N, 116°68′ E). One hybrid of maize was grown on April 28, 2019 and planted in rows 2.1 m long and 60 cm apart. A visible light sensor was mounted on a UAV and image data was acquired 20 days after sowing. The image capture system consisted of a 1-inch CMOS HD camera and an engineering-specific gimbal. The UAV flew at an altitude of 30 m, and the resolution of the captured images was 4000×3000 pixels. The data acquisition process is shown in Figure 1c.
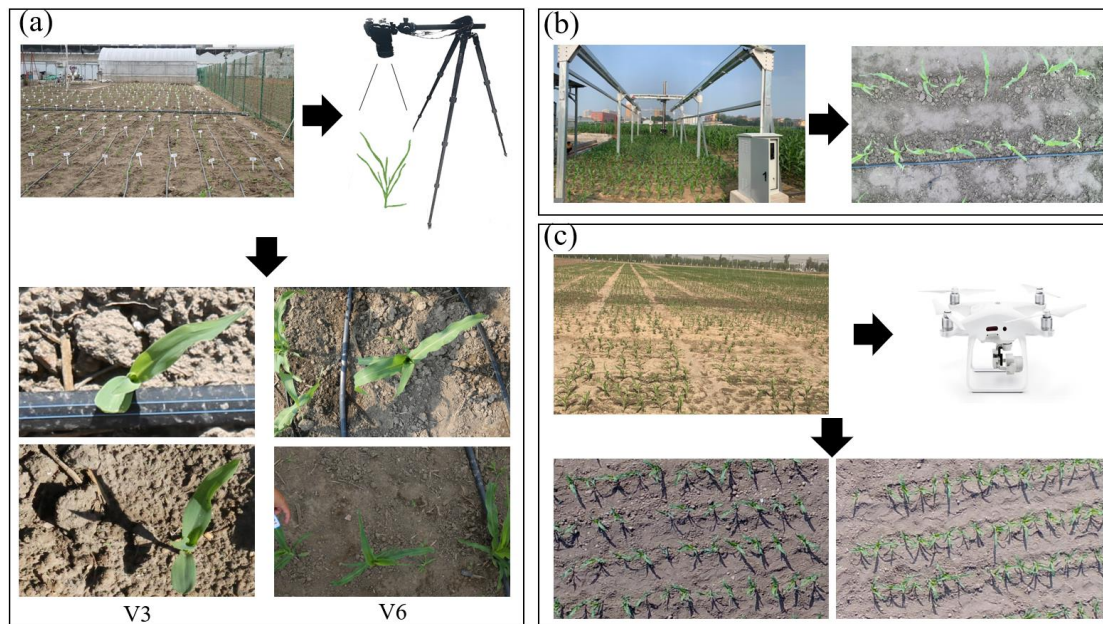
Figure 1. The set up for acquiring the photographs and examples of acquired images. This includes acquisition of top-view images using a tripod camera system (a), ground high-throughput phenotyping platform (b), and UAV platform (c).

Data Preparation

Datasets with annotated images are necessary for robust image segmentation models. In practice, this dataset was constructed using the top-view images obtained at two periods, V3 and V6 (Figure 1a). Because the soil background accounts for a large proportion of the raw images, the images were cropped around the area containing the plants and the images were scaled to 256×256 pixels for further training the model. A total of 192 images, containing seedling maize shoots, were annotated using LabelMe software. Among the total number of images, 128 images were expanded into 512 images to use as a training set after mirror symmetry, translation, and rotation. The remaining 64 labeled images were used to form a validation set to determine the criteria that may prevent network training. To prevent overfitting, the network will train until the losses on the validation set are stable. The model designed in this study is a small sample learning model, and data augmentation was adopted to ensure the quality of the training set, which will be discussed later. There are 200 images in the testing set, which were randomly selected from the four maize subpopulations described in the experiment in Figure 1a. Here, images of 50 hybrids belonging to each subpopulation were randomly selected (subpopulation SS consisted of only 32 hybrids, so there are 18 duplicated hybrid images belonging to the SS subpopulation in the test set).

PlantU-net Segmentation Network

To accurately segment maize shoots at the seedling stage in field conditions from the top-view image, the shoots were segmented as the foreground and output as a binary image. However, top-view images of field maize are relatively complex with stochastic background and uneven light conditions. Consequently, existing models are not satisfactory to extract pixel features. To address this issue, we built a PlantU-net segmentation network by adjusting the model structure and key functions of U-net [37], which improves the segmentation accuracy of images taken under a complex environment.

Model Structure

PlantU-net is a network designed for the segmentation of top-view images of crops grown in the field. A full convolution network is adopted to extract hierarchical features via an "end-to-end" process. As shown in Figure 2, the feature contraction path is composed of three layer downsampling modules, each module uses a 3×3 convolution to extract one row feature, and a 2×2 pooling operation to reduce the spatial dimensionality. Two convolution operations are conducted after downsampling to adjust the input size of the extended path. Corresponding to the contracted path, the extended path includes three layer upsampling modules. In each upsampling module, a 2×2 up sampling convolution is first performed to expand the spatial dimension. Then the upsampled results are fused with the low-level feature maps in the corresponding contracted path to connect contextual information across adjacent levels. Two convolution operations are performed during the upsampling process to reduce the feature dimension and facilitate feature fusion. After upsampling, a 1×1 convolution is performed as the full connection layer to output the segmented image. The same padding is filled in the samples during the convolution operations, which facilitates the computation. The parameters used for each layer of the model are shown in Table 1.
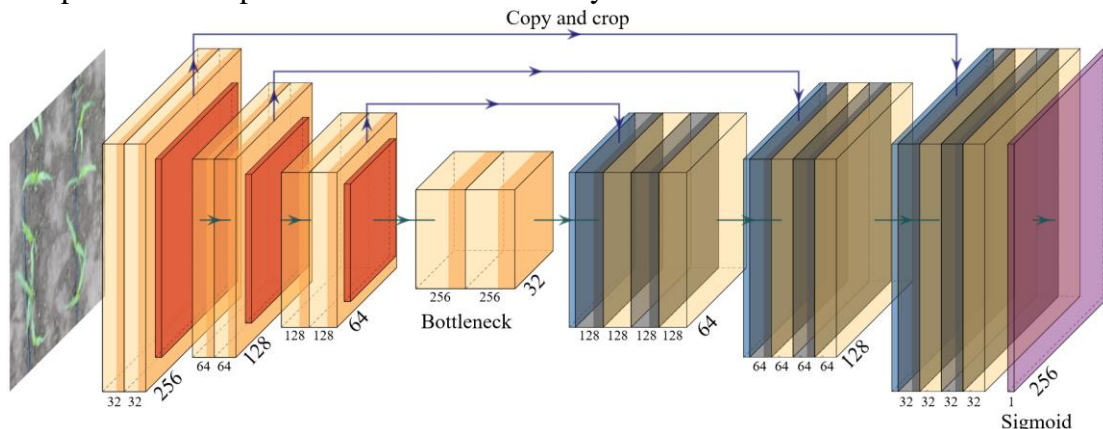
Figure 2. Architecture of the PlantU-net network. The input is a 256×256×3 image. The hidden layer of the network includes downsampling (left) and upsampling stages (right). Both stages comprise convolution (Conv),

203 activation (Leaky ReLU), and max pooling operations. The output is a 256 ×
204 256 × 1 segmented image.

205 **Table1. Configuration of the model structure parameters.** Refer to Figure
206 3 for the architecture of the PlantU-net network.

Layers	Input	Convolution filter	Output
Downsampling module 1	256×256×3	3×3×32	128×128×32
Downsampling module 2	128×128×32	3×3×64	64×64×64
Downsampling module 3	64×64×64	3×3×128	32×32×128
Convolution module	32×32×128	3×3×256, 3×3×128	32×32×128
Upsampling module 1	32×32×128	3×3×128, 3×3×64	64×64×64
Upsampling module 2	64×64×64	3×3×64, 3×3×32	128×128×32
Upsampling module 3	128×128×32	3×3×32	256×256×32
Convolution 1×1	256×256×32	3×3×1	256×256×1

207 To a certain extent, the network parameters of the model are reduced to ease the
208 burden of computers, and also to reduce the training time while ensuring the
209 segmentation effect. Since the number of training samples is small, a dropout layer is
210 appropriately added to prevent overfitting. In addition, to identify and utilize edge
211 features, a maximum pooling layer is adopted for downsampling.

212 ## Main Functions

213 ### Activation Function

214 The activation function in deep learning incorporates nonlinear factors to solve the
215 linear classification problem. In PlantU-net, Leaky ReLU is used as the activation
216 function. It still has an output when the input is negative, which eliminates the neuron
217 inactivation problem in back propagation. The expression is:

$$f(x) = \begin{cases} x & if\ x \geq 0 \\ \theta x & if\ x < 0 \end{cases} \tag{1}$$

218 For the final output layer of the model, Sigmoid is used as the activation function
219 for biclass. Sigmoid is capable of mapping a real number to an interval of (0, 1), and is
220 applicable for biclassing. Its expression is:

$$S(x) = \frac{1}{1 + e^{-x}} \tag{2}$$

221 ### Loss Function

222 The loss of function in the U-net model is replaced by the binary-cross-entropy
223 function in the PlantU-net model. The binary-cross-entropy function is a cross-entropy
224 of two-class classifications, which is a special case of the entropy function. The binary
225 classification is a logistic regression problem and the loss function of the logistic

226 regression can also be applied. Considering the output of the last layer of the sigmoid
227 function, this function is selected as the loss function. The mathematical expression of
228 binary-cross-entropy function is:

$$L = -[ylogy' + (1 - y) \, log(1 - y')] \tag{3}$$

229 where y is the true value and y' is an estimation when y = 1.

$$L = -logy' \tag{4}$$

230   The output of this loss of function is smaller when the estimated value is closer to
231 0, and the output value of the loss of function is larger when it is closer to 1. This is
232 suitable for the binary classification output of the last layer in this network.

Network Training

234   The PlantU-net was trained using the Keras framework (Figure 1) with
235 acceleration from GPUs (NVIDIA Quadro P6000). Five hundred and twelve images
236 were used to train the model. Data expansion is the key to making the network have the
237 required invariance and robustness because this model uses a small number of samples
238 for training. For top-view images of maize shoots, PlantU-net needs to meet the
239 robustness of plant morphology changes and value changes of gray images. Increasing
240 the random elastic deformation of training samples is the key to training segmentation
241 networks with a small number of labeled images. Therefore, during the data reading
242 phase, PlantU-net uses a random displacement vector on the 3 × 3 grid to generate a
243 smooth deformation, where the displacement comes from a Gaussian distribution with
244 a standard deviation of 10 pixels. Because the number of training samples is small, the
245 dropout layer is added to prevent the network from overfitting. Through these "data
246 enhancement" methods, the model performance is improved and overfitting is avoided.
247 In each epoch, the batch size was 1, the initial learning rate was 0.0001, and adam is
248 used as an optimizer to quickly converge the model. PlantU-net was trained until the
249 model converged (the training loss was satisfied and remained nearly unchanged).

Evaluation of segmentation accuracy

251   Because the segmentation of the top-view images of maize shoots using the
252 PlantU-net model is considered a binary classification problem, when evaluating the
253 segmentation results, the classification results of predicted output and ground truth
254 (GT) data can be used to perform pixel-level comparisons. If the pixel in the leaves is
255 marked as 1, and in the segmented image, the corresponding pixel is still 1, then it is
256 judged as true positive (TP); if the pixel point is judged as 0 after segmentation, the
257 pixel is judged as false positive (FP). Similarly, when the pixel in the original image
258 does not belong to the maize leaf, it is marked 0, if such pixel is judged as 1 after
259 segmentation, it is a false negative (FN); if such a pixel is also judged as 0, then it is a

true negative (TN). Following these rules, four indicators for evaluation [39] were used in this study:

(1) Precision. Precision represents the proportion of true positive samples among those predicted to be positive and is defined as:

$$P = \frac{TP}{TP + FP} \tag{5}$$

(2) Recall. Recall indicates how many positive samples of the total sample are correctly predicted and is defined as:

$$R = \frac{TP}{TP + FN} \tag{6}$$

(3) F1-Score. After calculating the accuracy and recall, the F1-Score can be calculated, which represents the weighted harmonic average of accuracy and recall. It is used for standardized measurement and is defined as:

$$F1 - Score = \frac{2PR}{P + R} \tag{7}$$

(4) DICE. Several metrics are commonly used to evaluate the segmentation results. Here, Rseg is used to present the predicted results, and Rgt represents the manually segmented ground truth data. Then DICE ($\in$[0,1]) is defined as:

$$DICE = \frac{2(R_{seg} + R_{gt})}{R_{seg} + R_{gt}} \tag{8}$$

DICE represents the ratio of the coincidence area between the segmentation results and the ground truth data to the total area. The value for perfect segmentation is 1.

Extraction of Phenotypic Parameters

The phenotypic traits concerning the shape and color characteristics of each shoot were estimated using PlantU-net based on the top-view images of the segmented maize shoots. The segmented images may still contain multiple maize plants. The phenotypic parameter extraction process will start with edge detection based on the segmentation results, connective domain markers based on the edge detection results, and finally single-plant phenotypic parameter extraction based on these connective domain markers.

Morphological feature extraction

The description of morphological features can be divided into two categories. The first category is the outline-based shape description, which focuses on describing the outline of the target area. The other category is the area-based shape description, which describes the target by area, geometric moment, eccentricity, and region shape. In this study, the center point Figure 3b) and contour (Figure 3c) of a maize shoot were first extracted from the segmented image. The minimum circumscribed radius (Figure 3d)

289 and aspect ratio (Figure 3e) of the plant were then calculated based on the extracted
290 contour. The coverage and plant azimuth plane were obtained based on the target region
291 in the segmented images as described below.
292 (1) The circumcircle radius (r) is half of the distance between the two pixels with the
293 furthest outline of the plant (Figure 3d):

$$r = \frac{max[dis(C_i, C_j)]}{2} \tag{9}$$

294 where C_i, C_j represent two pixels that are the furthest apart on the outline of the plant.
295 (2) The aspect ratio (A) is the ratio of the length to width in the minimum bounding box
296 of the plant (Figure 3e):

$$A = \frac{L}{H} \tag{10}$$

297 where L is the length in the x direction of the smallest bounding box and H is the length
298 in the y direction. The smallest bounding box refers to the smallest rectangle among the
299 n rectangles that can include the target plant area.
300 (3) The segmented results are binary images; thus, the maize shoot coverage (C) is
301 calculated by counting the total number of pixels occupied by the target area:

$$C = \sum_{x=0}^{m-1} \sum_{y=0}^{n-1} f(x, y) \tag{11}$$

302 where f (x, y) represents the binary map, m is the maximum number of pixels in
303 the x-axis direction, and k is the maximum number of pixels in the y-axis direction.
304 Regarding the binary maps, pixels of the target plant are always labeled by 1, whereas
305 the background pixels are labeled using 0 for the output; therefore, the pixel method of
306 calculation was used, meaning that pixels were counted as $f(x, y) = 1$ pixels.
307 Calibration objects were used in the original image of the dataset. The length and width
308 of the cropped image can be calculated using the calibration objects because the image
309 size was cropped to 256×256. The area of each pixel was calculated according to the
310 length and width of the image, and the size of the maize plant in the image was obtained
311 by multiplying the total number of pixels in the segmented target area.
312 (4) Studies have shown that expanded leaves of maize shoots are distributed along a
313 vertical plane, which is the plant azimuth plane [40,41]. The original images for this
314 study were oriented eastward during the data acquisition process; thus, the left side of
315 the image in the dataset indicates the north. In the Figure 3f, the blue line indicates a
316 single maize plant after segmentation and shows a north–south orientation. A red line
317 was fitted by clustering in the leaf section (or tangent to it if the clustering result is a
318 curve) as the plant azimuthal plane. The angle between the red line and the blue line
319 was calculated as β, which was used as the azimuthal plane angle of the plant. The
320 specific morphological features were extracted as shown in Figure 3.
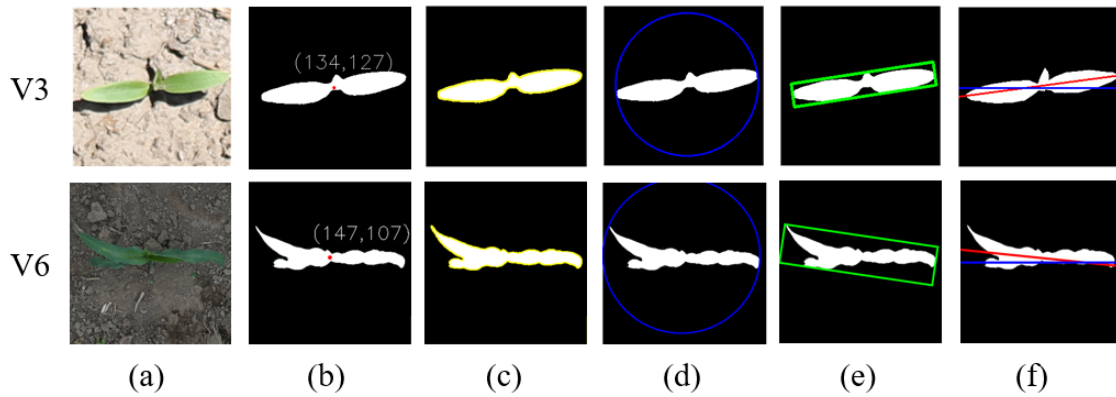
Figure 3. Illustration of phenotype extraction based on the image segmentation results of V3 and V6 growth stages, respectively. (a) The original image. (b) Coordination of the extracted center point. (c) Outline of the plant. (d) Minimum circumscribed circle. (e) Minimum bounding box. (f) Angle between the plant azimuth plane and the north. The red line represents the fitted azimuth plane and the blue line indicates the north–south direction. β is the angle between the red line and the blue line, and the value is between 0 and 180°. The angle β between the red and blue lines was estimated and used to represent the angle of the plant azimuthal plane (Figure 3f).

Extraction of color features

Maize leaf color has a direct relationship with moisture, nutrients, and disease, so color characteristics are an important parameter for plant phenotyping [41]. The pixels in the image are composed of red (R), green (G), and blue (B) values. By aligning the segmented image as a region of interest (MASK) with the original image, the RGB parameters of the color features of the MASK region can be extracted, which can further be transformed into HSV color space parameters [42]. This approach was primarily used because the HSV model is similar to the color perception by the human eye, and the HSV model can reduce the effect of light intensity changes on color discrimination. Therefore, the parameters of the color phenotypes in this study are represented using the mean of the RGB or HSV parameters.

Statistical analysis

The phenotypic traits extracted from segmentation results were compared with a manually measured value. The measured value of the circumcircle radius, aspect ratio, and plant azimuth plane was manually measured from the results by segmentation. Maize shoot coverage compared the segmentation results of PlantU-net with the results of manual segmentation. The adjusted coefficient of determination (R^2) and normalization root-mean-squared error (NRMSE) were calculated to assess the accuracy of these extracted parameters. The equations were as follows:

$$R^2 = 1 - \frac{\sum_{i=1}^{N}(vi - v'i)}{\sum_{i=1}^{n}(vi - \hat{v}i)^2} \tag{12}$$

$$NRMSE = \frac{\sqrt{\frac{1}{n}\sum_{i=1}^{N}(v_i - v'_i)^2}}{\hat{v}_i} \tag{13}$$

where n is the numbers of objects, vi is the results of manual segmentation, $v'i$ is the value of PlantU-net, and $\hat{v}_i$ is the mean value of the results of manual segmentation.

In the phenotypic analysis of the four subpopulations, this study analyzed the phenotypic trait data extracted from the test set. Box plots were drawn using Python. The extracted phenotypic trait data was marked in Excel and Python was used to write a program to read the data. The data was then visualized by calling the Matplotlib development library in Python.

Results

Model Segmentation Effect

The PlantU-net segmented network has been trained many times. During the training process, each epoch contained 200 batches with the size of 1, and the final training loss was shown in Figure 4. Training losses declined quickly in the first 100 batches (Figure 4), and then became slower. The loss for the final partition is 0.003. The model was trained on a workstation (2 Intel Xeon (R) Gold 6148 CPU, 256 GB RAM and NVIDIA Quadro P6000 GPU) for 41 minutes.
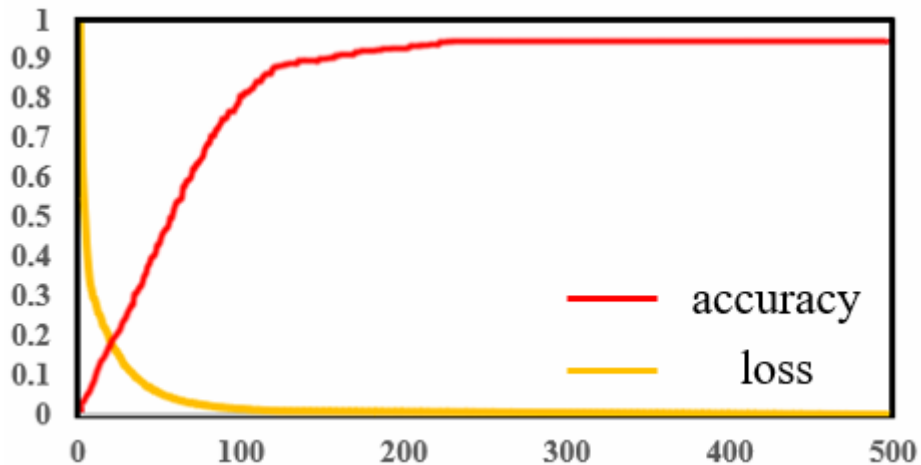
Figure 4. Training loss curve within 500 epochs and prediction precision

To show the image segmentation of the PlantU-net model of a single maize plant, the dataset and training parameters used by the PlantU-net model were imported into the U-net model for training, and the segmentation results of the two methods were compared with the manual segmentation results (Figure 5). The segmentation of the PlantU-net model is better than that of the U-net model. PlantU-net has a more complete

372 edge detection of segmentation results, and the precision of pixel classification of the
373 interested regions is higher.
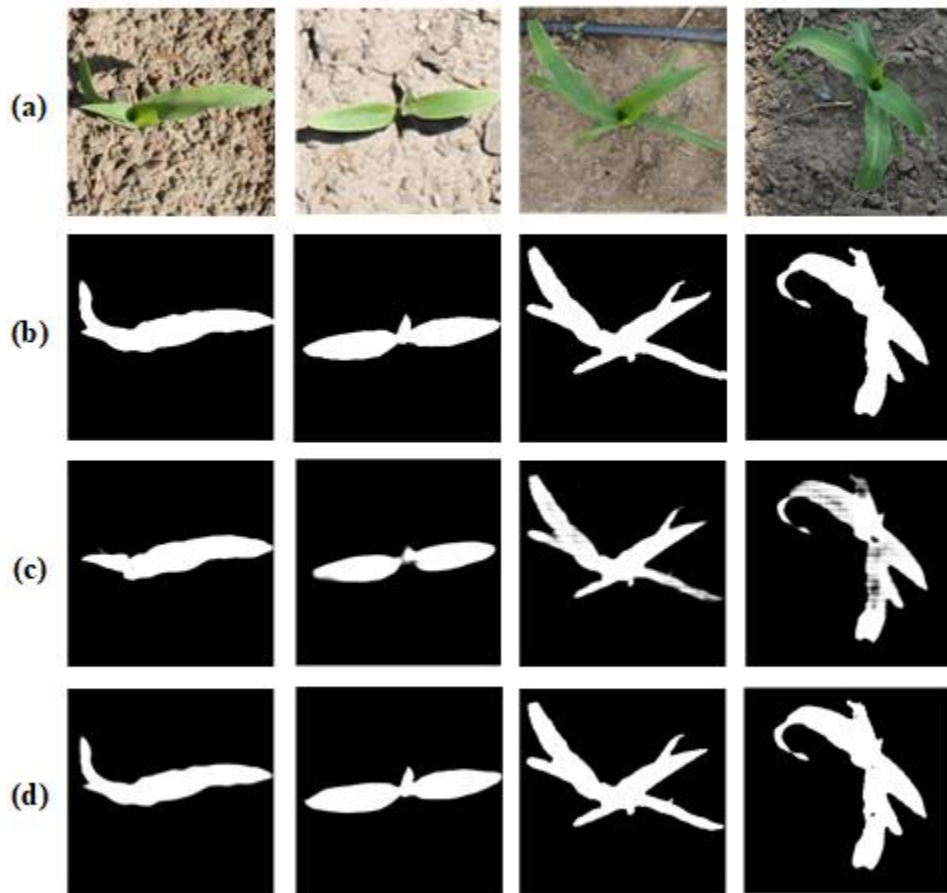
375 **Figure 5. Result of model segmentation**, in which (a) is the original image,
376 (b) is the ground truth by manual segmentation, (c) is the result obtained using
377 the U-net model, and (d) is the result obtained using the PlantU-net model.

378 **Table 2. Comparisons of the segmentation results of the U-net model and**
379 **the PlantU-net model using the data obtained from the validation set (V)**
380 **and test set (T).**

Segmentation method	Training time/M	Precision		Recall		F1-Score		DICE	
		V	T	V	T	V	T	V	T
U-net	52	0.87	0.86	0.86	0.90	0.86	0.88	0.87	0.86
PlantU-net	41	0.95	0.96	0.98	0.98	0.96	0.97	0.96	0.97

381 Table 2 compares the training time and segmentation results obtained using the
382 PlantU-net and U-net models. The segmentation precision of the PlantU-net model is
383 significantly higher than that of the U-net model, and less training time is required. In
384 the segmentation results of the PlantU-net model, the values of the verification set and
385 test set are similar. The PlantU-net model in the test set has a good segmentation effect,
386 with the precision (P) of the segmentation results reaching 0.96, recall rate (R) reaching
387 0.98, and F1-score reaching 0.97.

Individual Plant Scale Phenotypic Parameter Extraction

Using the PlantU-net model and the phenotype extraction method, the coverage, circumscribed radius, aspect ratio, and plant azimuth plane were determined using the validation dataset, and the measured data were compared with the extracted results for verification (Figure 6). Among them, the correlation coefficient R^2 of the artificial segmentation results and the automatic extraction results of the four morphological phenotypic parameters were all greater than 0.96, and the NRMSE values were all less than 10%, indicative of the reliability of the PlantU-net segmentation model and the phenotypic extraction method.
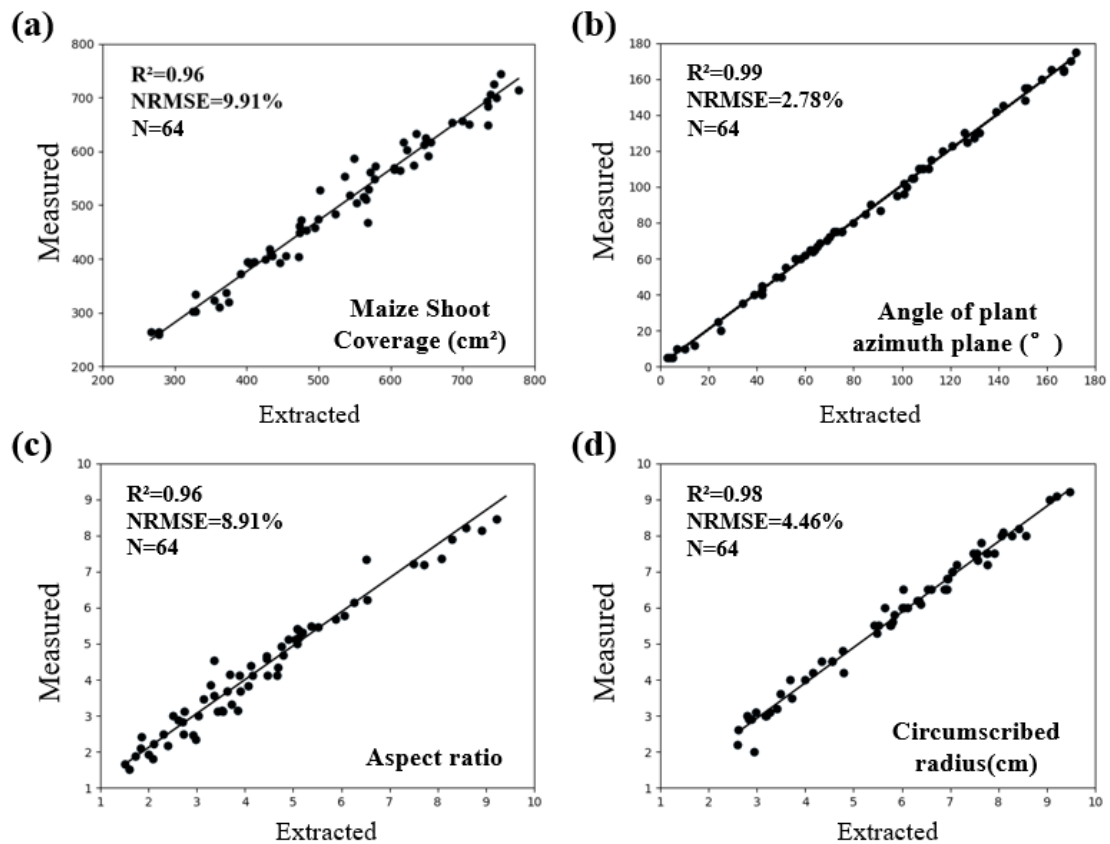
Figure 6. Correlation analysis between phenotypic measurements and manual measurements in top-view segmentation results of field maize. (a) Coverage, (b) the angle of plant azimuth plane, (c) aspect ratio, and (d) circumscribed radius

Population Scale Phenotypic Parameter Extraction

To evaluate the performance of the PlantU-net model in the image segmentation and phenotypic parameter extraction of the maize population, the field high-throughput phenotypic platform and the top-view of maize seedlings obtained by UAV were selected as inputs. The top-view images were obtained using both the field ground

407 phenotypic platform and UAV. Figure 7 shows the segmentation results and schematic
408 diagram of phenotypic parameter extraction of the PlantU-net model applied to two
409 sample plots.

410
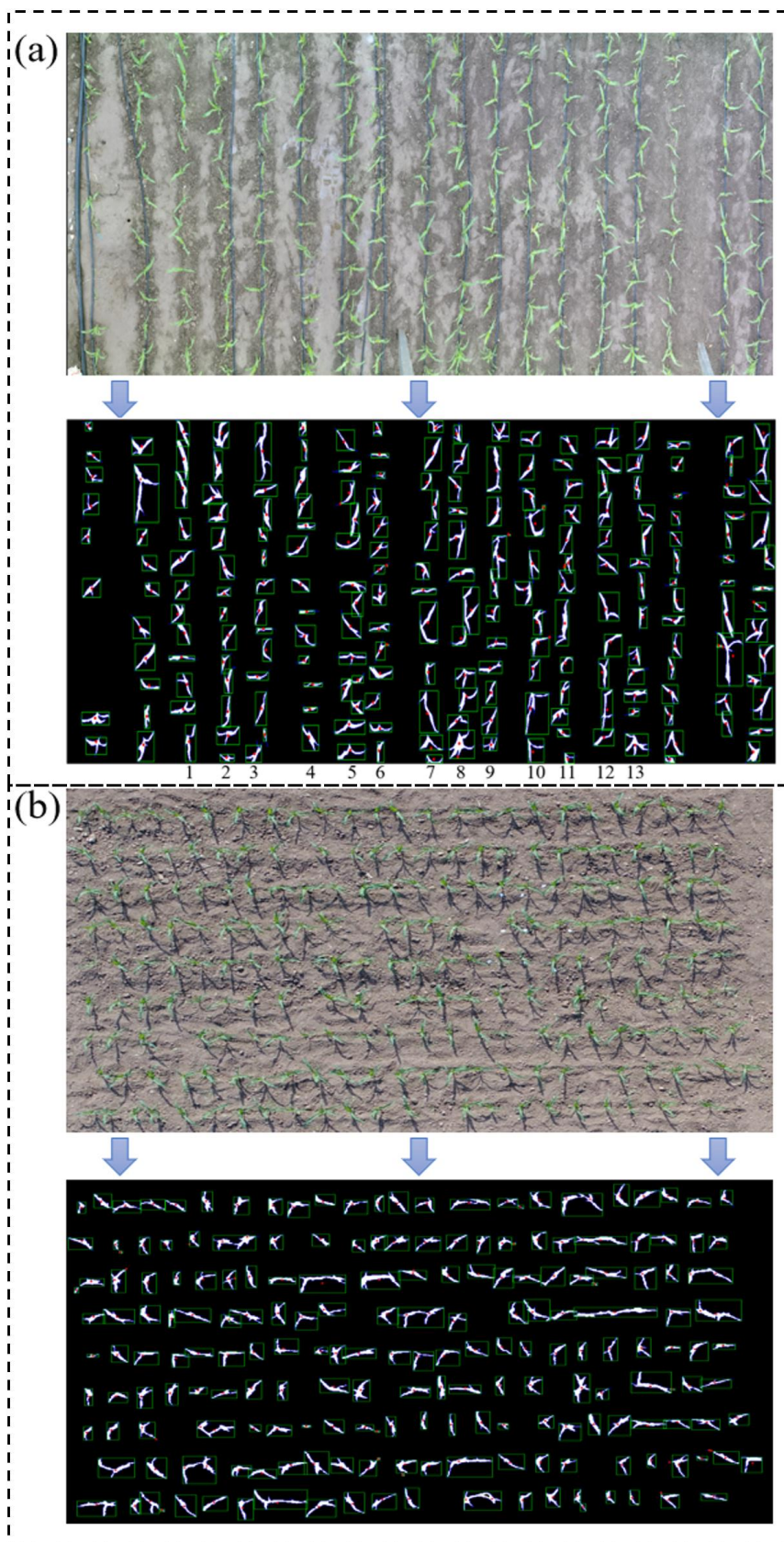
411 **Figure 7. Schematic diagram of the segmentation and phenotype**
412 **extraction of the top-view of maize seedlings obtained using the field**
413 **ground phenotyping platform and UAV.** In (a), a field track phenotypic
414 platform was used to obtain the top-view images. In addition to the protected
415 rows, a total of 13 varieties of maize plants were included (marked with a serial
416 number in the figure). (b) For the top-view of the maize population obtained
417 using the UAV, the image contains 216 maize plants of the same cultivar.

418 Phenotypic parameters were extracted from the segmentation results of two
419 sample plots using the above methods. The mean value and standard deviation of
420 various morphological parameters of the same cultivar of maize are shown in Table 3.
421 The mean value can be used to quantify the growth potential of different maize cultivars
422 in the same growth period, while the standard deviation can be used to evaluate the
423 consistency of plant growth within the same maize cultivar. Therefore, this method can
424 provide techniques for quantitative evaluation of plant growth potential, allowing for
425 phenotypic analysis of the top-view of a maize population at the seedling stage obtained
426 using multiple high-throughput phenotyping platforms in the field.

427 **Table 3. Morphological parameters of different maize cultivars.** AD268-
428 M751 in the table corresponds to 1–13 in figure 7A from top to bottom, and
429 the bottom row of the data is obtained from the phenotypic parameters of
430 maize plants in the image obtained by UAV.

Cultivar	Coverage (cm^2)		Aspect ratio		Circumscribed radius (cm)		Angle of plant azimuth plane (°)	
	AVG	STD	AVG	STD	AVG	STD	AVG	STD
AD268	132.23	42.28	5.73	2.34	9.88	1.92	101.00	53.11
MC670	150.44	45.41	4.13	2.08	10.73	2.21	85.30	45.68
JNK2010	130.55	42.75	5.49	1.40	10.69	1.67	97.40	49.95
JNK728	120.08	34.45	3.53	1.00	10.27	2.08	99.90	37.42
NK815	117.45	50.69	5.30	2.60	9.03	1.64	87.90	55.44
JKQC516	120.28	42.96	5.58	2.26	10.58	1.75	81.20	54.08
SK567	119.87	53.66	5.54	2.58	9.23	1.29	74.90	51.28
Y968	116.10	43.79	5.08	2.38	11.05	2.48	64.00	42.44
MC141	119.04	38.42	6.07	2.01	10.79	1.71	101.90	59.28
ZD958	103.31	45.97	6.17	1.94	11.13	2.16	94.90	53.55
XY335	105.82	36.95	5.43	1.98	11.99	1.72	106.80	48.16
JK968	112.15	45.98	4.86	2.44	10.28	2.08	87.40	51.96
M751	150.84	44.48	4.77	2.69	10.63	2.42	92.30	52.82
JNK728	115.92	37.41	5.35	2.08	7.97	1.47	89.57	49.42

431 # Phenotypic Analysis among Subpopulations

432 Phenotypic parameters were extracted from the images of the test set, and four

phenotypic parameters, including coverage, the angle of plant azimuth plane, aspect ratio and circumscribed radius were statistically analyzed from the perspective of subgroups. Figure 8 shows the results from the phenotypic parameter analysis extracted from the image segmentation results of the test set. Among the four subgroups there were no statistical differences between the azimuth plane of plant growth and the included angle of due north (Figure 8b), while the other three phenotypic parameters all had differences within subgroups. In the analysis of the other three phenotypic parameters, the extracted values of SS and NSS subgroups were similar, which was related to the temperate zone of the two groups of cultivars. The TST subgroup includes tropical and subtropical cultivars, so the extracted parameters are different from the SS and NSS subgroups. However, the differences of the Mixed subgroup are relatively distinct. The results of the coverage analysis (Figure 8a) shows that the coverage value of the Mixed subgroup in the test set is low; in contrast, the results of the circumscribed radius (Figure 8d) showed a higher extracted value for the Mixed subgroup than that of the SS and NSS subgroups. This indicates that the leaves of the Mixed subgroup are more slender, resulting in low plant coverage and high leaf extension during the same growth period.
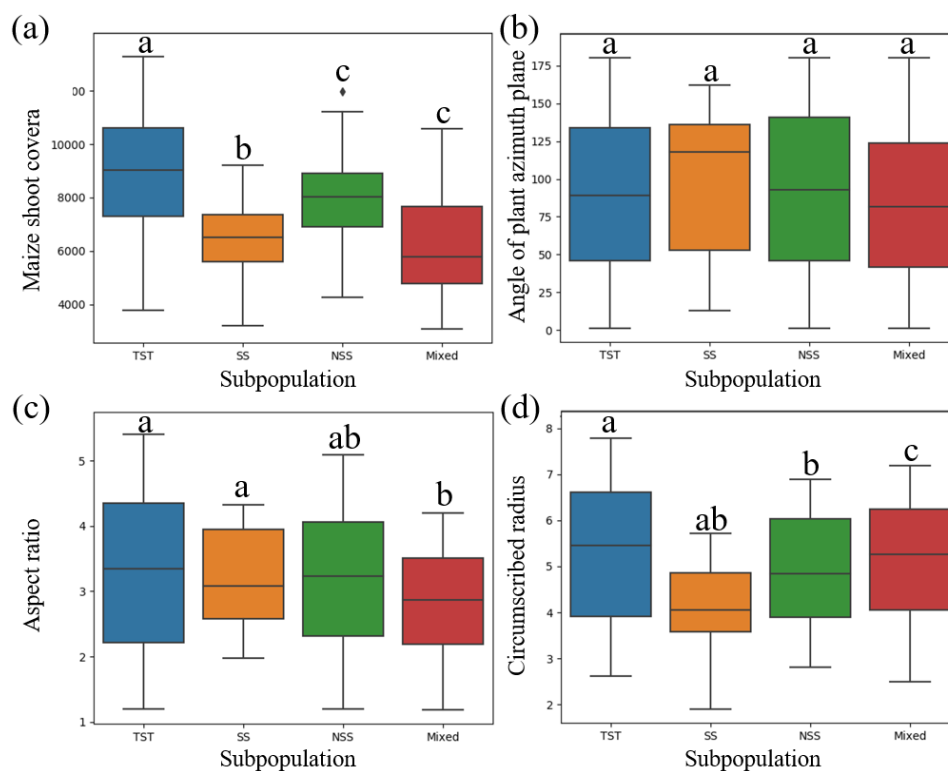
Figure 8. Various phenotypic parameters were analyzed based on the differences of different subgroups, in which the absence of shared letters indicated that the numerical differences of phenotypic parameters among subgroups were statistically significant ($P<0.05$). (a) Coverage, (b) the angle of plant azimuth plane, (c) aspect ratio, (d) circumscribed radius.

In terms of color phenotype, RGB and HSV phenotypic traits were extracted from the top image of the plant. Considering the segmented mask region is composed of

many pixels, the mean value of the color of the pixels in the region is taken as the color phenotypic parameter of the plants. Similarly, based on the spatial color information of RGB and HSV, color traits of maize plants of different subgroups were analyzed (Figure 9). According to the analysis of RGB values, there was no obvious difference among the subgroups of all cultivars. In the analysis based on HSV color information, the TST and NSS subgroups did not show evident differences in color; however, the color difference between the TST and NSS subgroups was clear (the H and S of the cultivars in the NSS subgroup were higher than those in the TST subgroup). Approximately 1/3 of cultivars in both the SS subgroup and the Mixed subgroup were different from other cultivars in this subgroup (both H and S were higher than other cultivars in this subgroup).
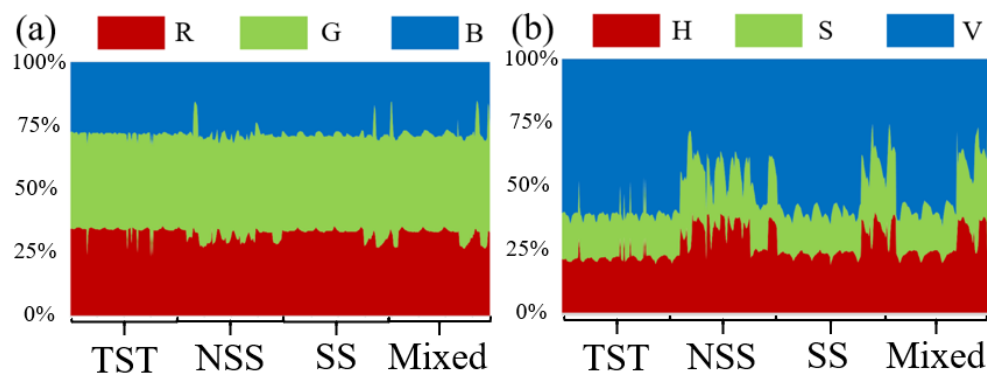
Figure 9. Waterfall diagram of foreground plants in top-view images of maize plants of different subgroups. (a) RGB mean value analysis, (b) HSV mean value analysis.

The above results indicated that the PlantU-net model and phenotypic trait extraction method could be used to quantitatively analyze the morphological and color phenotypic trait differences among subgroups, which was suitable for a correlation analysis of genotype–phenotype.

Discussion

Image Segmentation

At present, the threshold segmentation method is often used to segment top-view images of field crops. Although threshold segmentation with specific constraints can achieve very similar segmentation results [39,43], threshold segmentation is sensitive to noise and the effect on target segmentation is not ideal when there is little difference in gray scale. Threshold segmentation in different application scenarios (such as light and soil background) is relatively dependent on the selection of an empirical threshold. Manually setting different thresholds will greatly increase the workload of the

interaction of the segmentation process, and it is difficult to achieve high-throughput in the processing of large quantities of data [44,46]. In comparison, this study designed the PlantU-net network model, which can implement end-to-end seedling stage of maize and group top-view as segmentation with the average segmentation precision of P=0.96 and strong robustness. Under different light conditions and complex background features (the images used in this study have different background complexity, including weeds, drip irrigation, dry soil, and moist soil (Figure 1), different growth periods, and complex light environments (Figure 5 a)), accurate segmentation results were obtained without any human input. In addition, it only takes 0.04 s to extract various phenotypic parameters from the overhead image of a single maize plant (Figure 3) using PlantU-net. Moreover, it is only 0.6 s to extract phenotypic parameters from the top-view image of a population. The model can achieve high-throughput phenotypic parameter extraction on the premise of ensuring segmentation precision.

Compared with other algorithms that use deep learning for image segmentation, the PlantU-net model can improve the segmentation precision by 10% compared with the U-net model [37] (Table 2), indicating that the PlantU-net model has higher credibility in the application of top-view images segmentation of maize plants at the seedling stage. The method proposed by Orsolya Dobos et al. [45] uses U-net and 2,850 images to train the Arabidopsis image segmentation model, while the PlantU-net model only needs 512 images for training and the training data does not need complex pre-processing, indicating that PlantU-net achieves high-precision segmentation with less training data. Therefore, when PlantU-net is used to solve image segmentation problems in other crops at the seedling stage, only a small number of annotated images are needed, indicating that the method is highly scalable. Yanan Li et al. [53] proposed a method called DeepCotton to deal with the segmentation of cotton in the field from coarse to fine. First, the fully convolutional neural network (FCN) was used for the end-to-end segmentation of self-collected field images. After extraction of network features, the "UP" algorithm is proposed to correct the defects in the image. This method sacrifices processing efficiency by ensuring segmentation precision; the processing time of this method is approximately 6 s, whereas using PlantU-net to segment a single image only requires approximately 0.6 s.

Phenotypic Analysis

Crop phenotype extraction based on data from top-view images is the main way to obtain phenotypes from high-throughput phenotyping platforms for many crops [14]. For example, Zhou et al. [39] extracted the phenotypic parameters of maize seedlings from the gray scale images collected by a UAV phenotyping platform through Otsu threshold segmentation and skeleton extraction methods. This method has a good segmentation effect on the overall image, but the extraction precision of the phenotypic traits of individual plants is limited. The correlation between the seedling emergence

determined using the plant-bearing plane statistics and the measured data is only $R=0.77–0.86$. In contrast, the PlantU-net segmentation network can not only segment the top-view image of a single maize plant at the seedling stage with high precision (Figure 5), but also extract phenotypic parameters with a higher correlation with measured data ($R^2>0.96$). The results show that the PlantU-net method can replace artificial measurement and threshold segmentation for quantitative extraction and evaluation of phenotypic traits.

The location and direction of the maize plant remains relatively unchanged, and the method overcomes the problem of the plants overlapping each other when viewed from above. Therefore, the information of plant growth and plant azimuth-plane angle extracted from the top-view image of a maize population can provide measured data driving 3-D modeling of a maize population [47] and light distribution calculation and analysis [48] in the later growth stages. At present, the technology and equipment of high-throughput phenotyping platforms [51], including UAV [49], vehicle-based [50], and track-type, are developing rapidly, allowing for the collection of phenotypic data throughout the whole growth period. PlantU-net can also be applied to phenotypically analyze the top-view of a crop population obtained by multiple phenotypic platforms and can solve problems such as continuous monitoring of plant selection, analysis of plant growth difference between different plots, and analysis of plant growth consistency within the same treatment. These collected data would provide practical technical means for field crop breeding and cultivation research [52].

This study showed the applicability of the PlantU-net model in the extraction of phenotypic parameters in the seedling stage of maize. However, due to a large number of cross-shading in the top-view images caused by the overlapping of different plant leaves, this model could not solve the problem of phenotypic extraction in the middle and late stage of maize plant growth and development. Future work must determine how to use top-view continuity and the edge detection ability of the PlantU-net model to achieve the phenotypic extraction of plants in the middle and late stages of crop plants.

Conclusion

In this study, an end-to-end segmentation method named PlantU-net was proposed based on the fully convolutional network, which improved the high-throughput segmentation performance of a top-view image of a seedling population and realized the accurate extraction of phenotypic data. The PlantU-net model had an average segmentation precision of 0.96 for the aerial image of maize plants at the seedling stage, and the phenotypic parameters extracted from the segmentation results were highly correlated with the values obtained by manual measurement ($R^2=0.96-0.99$). The model described in this manuscript is helpful for the segmentation of top-view images of the maize shoot, the extraction of phenotypes, and the quantitative evaluation of phenotypic

traits obtained by high-throughput UAV and ground phenotypic platforms.

References

1. Zhao, C.; Zhang, Y.; Du, J.; Guo, X.; Wen, W.; Gu, S.; Wang, J.; Fan, J. Crop Phenomics: Current Status and Perspectives. Front. Plant Sci. **2019**, 10, doi:10.3389/fpls.2019.00714.
2. Yang, W.; Feng, H.; Zhang, X.; Zhang, J.; Doonan, J.H.; Batchelor, W.D.; Xiong, L.; Yan, J. Crop Phenomics and High-Throughput Phenotyping: Past Decades, Current Challenges, and Future Perspectives. Molecular Plant **2020**, 13, 187-214, doi:10.1016/j.molp.2020.01.008.
3. Holman, F.; Riche, A.; Michalski, A.; Castle, M.; Wooster, M.; Hawkesford, M. High Throughput Field Phenotyping of Wheat Plant Height and Growth Rate in Field Plot Trials Using UAV Based Remote Sensing. Remote Sensing **2016**, 8, doi:10.3390/rs8121031.
4. Richard, C.A.; Hickey, L.T.; Fletcher, S.; Jennings, R.; Chenu, K.; Christopher, J.T. High-throughput phenotyping of seminal root traits in wheat. Plant Methods **2015**, 11, 13, doi:10.1186/s13007-015-0055-9.
5. Zheng, Y.Y.; Kong, J.L.; Jin, X.B.; Wang, X.Y.; Zuo, M. CropDeep: The Crop Vision Dataset for Deep-Learning-Based Classification and Detection in Precision Agriculture. Sensors (Basel) **2019**, 19, doi:10.3390/s19051058.
6. White, J.W.; Andrade-Sanchez, P.; Gore, M.A.; Bronson, K.F.; Coffelt, T.A.; Conley, M.M.; Feldmann, K.A.; French, A.N.; Heun, J.T.; Hunsaker, D.J. Field-based phenomics for plant genetics research. 133, 101-112.
7. Scharr, H. Leaf segmentation in plant phenotyping: a collation study. Machine Vision & Applications **2016**, 27, 585-606.
8. Das Choudhury, S.; Samal, A.; Awada, T. Leveraging Image Analysis for High-Throughput Plant Phenotyping. Front Plant Sci **2019**, 10, 508, doi:10.3389/fpls.2019.00508.
9. Velumani, K.; Oude Elberink, S.; Yang, M.Y.; Baret, F. Wheat Ear Detection in Plots by Segmenting Mobile Laser Scanner Data. ISPRS Annals of Photogrammetry, Remote Sensing and Spatial Information Sciences **2017**, IV-2/W4, 149-156, doi:10.5194/isprs-annals-IV-2-W4-149-2017.
10. Nguyen, T.T.N.; Le, T.-L.; Vu, H.; Hoang, V.-S.; Tran, T.-H. Crowdsourcing for botanical data collection towards to automatic plant identification: A review. Computers and Electronics in Agriculture **2018**, 155, 412-425, doi:10.1016/j.compag.2018.10.042.
11. Lu, H.; Cao, Z.G.; Xiao, Y.; Li, Y.A.; Zhu, Y.J. Region-based colour modelling for joint crop and maize tassel segmentation. Biosyst. Eng. **2016**, 147, 139-150, doi:10.1016/j.biosystemseng.2016.04.007.
12. Janssens, O.; Vylder, J.D.; Aelterman, J.; Verstockt, S.; Walle, R.V.D. Leaf

604	segmentation and parallel phenotyping for the analysis of gene networks in plants.
605	In Proceedings of European Signal Processing Conference (EUSIPCO).
606	13. Lièvre, M.; Wuyts, N.; Cookson, S.J.; Bresson, J.; Dapp, M.; Vasseur, F.o.;
607	Massonnet, C.; Tisné, S.; Bettembourg, M.; Balsera, C. Phenotyping the kinematics
608	of leaf development in flowering plants: recommendations and pitfalls. Wiley
609	Interdisciplinary Reviews Developmental Biology 2, n/a-n/a.
610	14. Praveen Kumar, J.; Domnic, S. Image based leaf segmentation and counting in
611	rosette plants. Information Processing in Agriculture **2019**, 6, 233-246,
612	doi:10.1016/j.inpa.2018.09.005.
613	15. Hamuda, E.; Glavin, M.; Jones, E. A survey of image processing techniques for
614	plant extraction and segmentation in the field. Computers and Electronics in
615	Agriculture **2016**, 125, 184-199, doi:10.1016/j.compag.2016.04.024.
616	16. Gehan, M.A.; Fahlgren, N.; Abbasi, A.; Berry, J.C.; Sax, T. PlantCV v2: Image
617	analysis software for high-throughput plant phenotyping. PeerJ **2017**, 5, e4088.
618	17. Yin, X.; Liu, X.; Chen, J.; Kramer, D.M. Joint Multi-Leaf Segmentation,
619	Alignment, and Tracking for Fluorescence Plant Videos. IEEE Transactions on
620	Pattern Analysis & Machine Intelligence **2015**, PP.
621	18. Alenya, G.; Dellen, B.; Foix, S.; Torras, C. Robotized Plant Probing: Leaf
622	Segmentation Utilizing Time-of-Flight Data. IEEE Robotics & Automation
623	Magazine 20, 50-59.
624	19. Kulikov, V.; Yurchenko, V.; Lempitsky, V. Instance Segmentation by Deep
625	Coloring.
626	20. Unseok, L.; Sungyul, C.; Anantrio, P.G.; Hyoungseok, K.; Hwan, K.D.; Hector, C.
627	An automated, high-throughput plant phenotyping system using machine learning-
628	based plant segmentation and image analysis. PLoS One 13, e0196615-.
629	21. Zhang, S.W.; You, Z.H.; Wu, X.W. Plant disease leaf image segmentation based on
630	superpixel clustering and EM algorithm. Neural Comput. Appl. **2019**, 31, 1225-
631	1232, doi:10.1007/s00521-017-3067-8.
632	22. Mahlein, A.K. Plant Disease Detection by Imaging Sensors - Parallels and Specific
633	Demands for Precision Agriculture and Plant Phenotyping. Plant Dis. **2016**, 100,
634	241-251, doi:10.1094/pdis-03-15-0340-fe.
635	23. Sekulska-Nalewajko, J.; Goclawski, J.; Chojak-Kozniewska, J.; Kuzniak, E.
636	Automated image analysis for quantification of reactive oxygen species in plant
637	leaves. Methods **2016**, 109, 114-122, doi:10.1016/j.ymeth.2016.05.018.
638	24. Wu, Q.; Sun, H.; Li, M.Z.; Song, Y.Y.; Zhang, Y.E. Research on Maize
639	Multispectral Image Accurate Segmentation and Chlorophyll Index Estimation.
640	Spectrosc. Spectr. Anal. **2015**, 35, 178-183, doi:10.3964/j.issn.1000-
641	0593(2015)01-0178-06.
642	25. Mochida, K.; Koda, S.; Inoue, K.; Hirayama, T.; Tanaka, S.; Nishii, R.; Melgani, F.
643	Computer vision-based phenotyping for improvement of plant productivity: a
644	machine learning perspective. Gigascience **2019**, 8,
645	doi:10.1093/gigascience/giy153.

26. Gao, L.W.; Lin, X.H. Fully automatic segmentation method for medicinal plant leaf images in complex background. Computers and Electronics in Agriculture **2019**, 164, 14, doi:10.1016/j.compag.2019.104924.

27. Barth, R.; Ijsselmuiden, J.; Hemming, J.; Van Henten, E.J. Synthetic bootstrapping of convolutional neural networks for semantic plant part segmentation. Computers and Electronics in Agriculture **2019**, 161, 291-304, doi:10.1016/j.compag.2017.11.040.

28. Chen, G.F.; Hu, J.; Li, D.L.; Si, X.L. Image Recognition of Maize Diseases Based on Fuzzy Clustering and Support Vector Machine Algorithm. Sens. Lett. **2012**, 10, 433-438, doi:10.1166/sl.2012.1882.

29. Ward, D.; Moghadam, P.; Hudson, N. Deep Leaf Segmentation Using Synthetic Data. **2018**, arXiv:1807.10931 [cs.CV], doi:arXiv:1807.10931 [cs.CV].

30. Lin, K.; Gong, L.; Huang, Y.; Liu, C.; Pan, J. Deep Learning-Based Segmentation and Quantification of Cucumber Powdery Mildew Using Convolutional Neural Network. Front Plant Sci **2019**, 10, 155, doi:10.3389/fpls.2019.00155.

31. Ma, X.; Deng, X.W.; Qi, L.; Jiang, Y.; Li, H.W.; Wang, Y.W.; Xing, X.P. Fully convolutional network for rice seedling and weed image segmentation at the seedling stage in paddy fields. PLoS One **2019**, 14, 13, doi:10.1371/journal.pone.0215676.

32. Ma, J.C.; Du, K.M.; Zheng, F.X.; Zhang, L.X.; Gong, Z.H.; Sun, Z.F. A recognition method for cucumber diseases using leaf symptom images based on deep convolutional neural network. Computers and Electronics in Agriculture **2018**, 154, 18-24, doi:10.1016/j.compag.2018.08.048.

33. Barbedo, J.G.A. Plant disease identification from individual lesions and spots using deep learning. Biosyst. Eng. **2019**, 180, 96-107, doi:10.1016/j.biosystemseng.2019.02.002.

34. Wang, G.; Sun, Y.; Wang, J.X. Automatic Image-Based Plant Disease Severity Estimation Using Deep Learning. Comput. Intell. Neurosci. **2017**, 10.1155/2017/2917536, 8, doi:10.1155/2017/2917536.

35. Zhou, C.; Ye, H.; Xu, Z.; Hu, J.; Shi, X.; Hua, S.; Yue, J.; Yang, G. Estimating Maize-Leaf Coverage in Field Conditions by Applying a Machine Learning Algorithm to UAV Remote Sensing Images. Applied Sciences **2019**, 9, doi:10.3390/app9112389.

36. Yang, X.; Gao, S.; Xu, S.; Zhang, Z.; Prasanna, B.M.; Li, L.; Li, J.; Yan, J. Characterization of a global germplasm collection and its potential utilization for analysis of complex quantitative traits in maize. Molecular Breeding **2010**, 28, 511-526, doi:10.1007/s11032-010-9500-7.

37. Ronneberger, O.; Fischer, P.; Brox, T. U-Net: Convolutional Networks for Biomedical Image Segmentation. arXiv:1505.04597v1 [cs.CV] **2015**.

38. Goutte, C.; Gaussier, E. A Probabilistic Interpretation of Precision, Recall and F-Score, with Implication for Evaluation. **2005**, 51, 952-952.

39. Zhou, C.; Yang, G.; Liang, D.; Yang, X.; Xu, B. An Integrated Skeleton Extraction

688   and Pruning Method for Spatial Recognition of Maize Seedlings in MGV and UAV
689   Remote Images. IEEE Transactions on Geoscience and Remote Sensing **2018**, 56,
690   4618-4632, doi:10.1109/tgrs.2018.2830823.
691 40.   Zhou, C.; Ye, H.; Xu, Z.; Hu, J.; Shi, X.; Hua, S.; Yue, J.; Yang, G. Estimating
692   Maize-Leaf Coverage in Field Conditions by Applying a Machine Learning
693   Algorithm to UAV Remote Sensing Images. Applied Sciences **2019**, 9,
694   doi:10.3390/app9112389.
695 41. Wen, W.L.; Guo, X.Y.; Zhao, C.J.; Xiao, B.X.; Wang, Y.J. Research on Maize Plant
696   Type Parameter Extraction by Using Three Dimensional Digitizing Data. Scientia
697   Agricultura Sinica **2018**.
698 42. Berry, J.C.; Fahlgren, N.; Pokorny, A.A.; Bart, R.S.; Veley, K.M. An automated,
699   high-throughput method for standardizing image color profiles to improve image-
700   based plant phenotyping. PeerJ **2018**, 6, doi:10.7717/peerj.5727.
701 43. Cinat, P.; Di Gennaro, S.F.; Berton, A.; Matese, A. Comparison of Unsupervised
702   Algorithms for Vineyard Canopy Segmentation from UAV Multispectral Images.
703   Remote Sensing **2019**, 11, 24, doi:10.3390/rs11091023.
704 44. Gocławski, J.; Sekulska-Nalewajko, J.; Kuźniak, E. Neural network segmentation
705   of images from stained cucurbits leaves with colour symptoms of biotic and abiotic
706   stresses. International Journal of Applied Mathematics and Computer Science **2012**,
707   22, 669-684, doi:10.2478/v10006-012-0050-5.
708 45. Dobos, O.; Horvath, P.; Nagy, F.; Danka, T.; András, V. A deep learning-based
709   approach for high-throughput hypocotyl phenotyping; 2019; 10.1101/651729.
710 46. Wang, Y.; Xu, L.H. Unsupervised segmentation of greenhouse plant images based
711   on modified Latent Dirichlet Allocation. PeerJ **2018**, 6, 31, doi:10.7717/peerj.5036.
712 47. Wen W.;Zhao C.;Guo X.;Wang Y.;Du J.;Yu Z. Construction method of three-
713   dimensional model of maize colony based on t-distribution function. Transactions
714   of the Chinese Society of Agricultural Engineering 2018; 10.11975/j.issn.1002-
715   6819.2018.04.023.
716 48.   Wen, W.; Guo, X.; Li, B.; Wang, C.; Wang, Y.; Yu, Z.; Wu, S.; Fan, J.; Gu, S.; Lu,
717   X. Estimating canopy gap fraction and diffuse light interception in 3D maize
718   canopy using hierarchical hemispheres. Agricultural and Forest Meteorology **2019**,
719   276-277, 107594, doi:https://doi.org/10.1016/j.agrformet.2019.05.025.
720 49. Gevaert, C.; Persello, C.; Vosselman, G. Optimizing Multiple Kernel Learning for
721   the Classification of UAV Data. Remote Sensing **2016**, 8, doi:10.3390/rs8121025.
722 50. Primicerio, J.; Gennaro, S.F.D.; Fiorillo, E.; Genesio, L.; Lugato, E.; Matese, A.;
723   Vaccari, F.P. A flexible unmanned aerial vehicle for precision agriculture. Precision
724   Agriculture 13, 517-523.
725 51. Andradesanchez, P. Development and evaluation of a field-based high-throughput
726   phenotyping platform. Functional Plant Biology **2014**, 41.
727 52. Yang, W.; Guo, Z.; Huang, C.; Wang, K.; Jiang, N.; Feng, H.; Chen, G.; Liu, Q.;
728   Xiong, L. Genome-wide association study of rice (Oryza sativaL.) leaf traits with
729   a high-throughput leaf scorer. Journal of Experimental Botany 2015, 66, 5605-

730   5615, doi:10.1093/jxb/erv100.

731 53. Li,Y.A.; Cao, Z.G.; Xiao, Y.; Cremers, A.B. DeepCotton: in-field cotton
732   segmentation using deep fully convolutional network. J. Electron. Imaging **2017**,
733   26, 14, doi:10.1117/1.Jei.26.5.053028.

734